

Effect of SrO Precursors on the Microstructure and Mechanical Properties of Zirconia-Toughened Alumina (ZTA) Composites

Jing Zhou¹, Shuhao Jiang^{2, 3}, Jinping Yang^{*2}, Teng Ma³, Jian Zhang^{*3}

¹Shanghai University of Medicine & Health Sciences, College of Medical Technology, Shanghai, 201318, China.

²College of Materials Science and Engineering, North China University of Science and Technology, Tangshan, 063210, China.

³State Key Laboratory of High Performance Ceramics and Superfine Microstructure, Shanghai Institute of Ceramics, Chinese Academy of Sciences, Shanghai 200050, China

received March 23, 2025; received in revised form June 1, 2025; accepted June 3, 2025

Abstract

In this study, ZTA (3Y-TZP/Al₂O₃) ceramic composites with added SrO sintering aid from SrCO₃ and Sr(NO₃)₂ precursors were prepared by means of pressureless sintering and hot isostatic pressing sintering (HIPing). The microstructure and mechanical properties of the ZTA ceramic composites with added SrCO₃ and Sr(NO₃)₂ were examined, respectively. It was found that SrO incorporation inhibited grain growth and induced the *in situ* formation of SrAl₁₂O₁₉ platelets. As the SrO content increased, the fracture toughness of the ceramic composites improved; additionally, the hardness and flexural strength initially increased and then decreased. Compared to ZTA ceramics with SrCO₃ addition, the samples with Sr(NO₃)₂ had finer grains with a more uniform platelet distribution. ZTA ceramic composites with the addition of Sr(NO₃)₂ exhibited a maximum hardness, four-point flexural strength, and fracture toughness of 18.46 GPa, 887 MPa, and 6.97 MPa·m^{1/2}, respectively.

Keywords: Ceramic composites, strontium hexaluminate, platelet, *in-situ* formation, mechanical properties

I. Introduction

Zirconia-toughened alumina (ZTA) is a ceramic composite with alumina as the matrix, and 3Y-TZP (zirconia contains 3 mol% Y₂O₃) as the toughening phase. The martensitic phase transformation of tetragonal zirconia contributes to the enhancement of fracture toughness¹ of ZTA ceramic composites. Due to their excellent chemical stability, wear resistance, and high strength, ZTA ceramic composites are widely used in industrial fields^{2–3}. However, the comprehensive performance of these single-phase-reinforced ceramics still does not meet the requirements for certain applications, such as hip joint implants. To further enhance the ceramic mechanical performance, researchers have pursued microstructural toughening by using a high aspect ratio of a second phase (whisker, fiber, and platelet). Unfortunately, sources of whiskers or fibers for ceramic composites are limited and expensive. Besides, introducing whiskers or fibers by means of mechanical ball milling leads to poor dispersion uniformity and difficulties in the densification process, which can also cause health issues. Therefore, more flexible and sustainable methods are needed. Recently, the addition of oxides to ceramic matrices has gradually become a popular research

topic due to the *in situ* formation of elongated grains of hexaaluminate.

Hexaaluminates exhibit high aspect ratios in crystal grains, such as needle-like⁴, rod-like⁵, and platelet^{6–7}. They contribute to improving the fracture toughness and flexural strength of ceramic materials through mechanisms such as transgranular cracking, crack deflection^{8–9} and crack bridging^{10–12}. During the sintering process, oxides (such as SrO, CaO, and La₂O₃)¹³ added into the ceramic matrix react with Al₂O₃, leading to *in situ* formation of platelet hexaaluminates (such as SrAl₁₂O₁₉¹⁴, CaAl₁₂O₁₉, and LaAl₁₁O₁₈). Among them, SrO has been used as an additive in CeramTec's products to improve mechanical properties. Flexural strength and fracture toughness of CeramTec's products were 1380 MPa and 6 MPa·m^{1/2}, respectively. A substantial amount of related research has been prompted. The addition of SrO is mostly derived from the decomposition of salts (SrCO₃ or Sr(NO₃)₂)¹⁵. By adding SrCO₃ to ZTA and allowing it to decompose into SrO oxide, Oungkulsolmongkol *et al.*⁸ successfully increased the fracture toughness of ZTA to 5.8 MPa·m^{1/2}. This finding was consistent with the results of Arab *et al.*¹⁶; in their research, the transgranular fracture became more significant as the SrCO₃ content increased, and the maximum fracture toughness was observed at a SrCO₃ content of 2.0 wt%. Using the sol-gel method, Naga *et al.*^{17–18}

* Corresponding author: Jinping Yang: imjp_yang@163.com
co-corresponding author: Jian Zhang: jianzhang@mail.sic.ac.cn

added different contents of SrCO_3 to ZTA to form elongated $\text{SrAl}_{12}\text{O}_{19}$ grains *in situ* and achieved a fracture toughness of $7.82 \text{ MPa}\cdot\text{m}^{1/2}$. Basha *et al.*¹⁹ proposed that $\text{Sr}(\text{NO}_3)_2$ ionizes into Sr^{2+} and NO_3^- ions in water, leading to a more uniform distribution of Sr^{2+} in ZTA than that of SrCO_3 incorporated by means of mechanical mixing. Therefore, they investigated the influence of SrO by using $\text{Sr}(\text{NO}_3)_2\cdot 6\text{H}_2\text{O}$ on the Al_2O_3 -5 wt% ZrO_2 ceramic system. Compared to those of the pure ZTA, the strength and toughness of the composite with the addition of 5 000 ppm SrO increased by 15 %.

The toughening effect of the ZTA ceramic composite is closely associated with the quantity of Y-TZP, grain size, and concentration of Y. Relatively speaking, due to the unique transformation toughening mechanism of zirconia, a higher proportion of zirconia brings the grain size closer to the critical grain size, thereby increasing toughness. When Y concentrations are lower, the transformation toughening mechanism is more readily activated, thus enhancing toughness and improving wear resistance. In the case of a fixed Al_2O_3 -to- ZrO_2 ratio, the introduction form of SrO, its quantity, and the formation of $\text{SrAl}_{12}\text{O}_{19}$ platelets directly impact the mechanical properties of the ZTA ceramic composite. However, research on the effects of different SrO precursor types on the microstructure and mechanical properties of ZTA ceramic composite is limited.

This paper selected SrCO_3 and $\text{Sr}(\text{NO}_3)_2$ as sintering aid precursors to prepare Sr-doped ZTA composite ceramics using a combined approach of pressureless sintering and hot isostatic pressing. The primary objective of this study was to systematically compare and investigate the comprehensive effects of SrO doping content (derived from different precursors) and its doping form on the densification process, microstructural evolution (particularly the formation mechanism and distribution of $\text{SrAl}_{12}\text{O}_{19}$ platelets), and mechanical properties of the ZTA composite materials. Furthermore, the mechanism by which the uniformity of platelet distribution influences mechanical properties was analyzed in depth, providing novel research perspectives for enhancing the mechanical performance of ZTA composite ceramics.

II. Experimental

(1) Sample preparation

Powders of 3Y-TZP (3 mol% Y_2O_3 , purity > 99.95 %, 40 nm; Tosoh, Japan), alumina (purity > 99.99 %, 170 nm; TM-DAR, TAIMEI, Japan), strontium carbonate (AR, 0.5–1 μm ; Aladdin, China), and strontium nitrate (AR, Sinpharm Chemical Reagent Co., Ltd., China) were used. The compositions of the materials used in this experiment are listed in Table 1. A mixture of 75 wt% alumina and 25 wt% 3Y-TZP powder was used as the initial composition of the ZTA. To prepare mixed powders of ZTA and SrO, $\text{Sr}(\text{NO}_3)_2$ and SrCO_3 were used as precursors. Different contents of $\text{Sr}(\text{NO}_3)_2$ and SrCO_3 were added to the ZTA. The samples with the addition of $\text{Sr}(\text{NO}_3)_2$ were named ZTA-SN25, ZTA-SN50, ZTA-SN75, and ZTA-SN10, while the samples with SrCO_3 were named ZTA-SC25, ZTA-SC50, ZTA-SC75, and ZTA-SC10, corre-

sponding to that the SrO contents in the samples were 0.25 wt%, 0.5 wt%, 0.75 wt%, and 1.0 wt%, respectively. $\text{Sr}(\text{NO}_3)_2$ and SrCO_3 were mixed with ZTA powder in isopropyl alcohol using a planetary ball mill for 24 hours. 3Y-TZP milling balls (5 mm in diameter) were used as milling media. The powder suspensions were continuously stirred and then dried on a heating plate at 80 °C to prevent uneven distribution due to sedimentation of 3Y-TZP and further air-dried at 90 °C for 12 h. To decompose the nitrate and carbonate, the mixed powders were calcined at 800 °C for 2 h at a heating rate of 5 K/min. All the calcined powders were sieved using an 80-mesh sieve. Green bodies were formed by means of die pressing at 37.5 MPa, followed by cold isostatic pressing (CIP) at 200 MPa. The green bodies subsequently underwent pressureless sintering at 1410 °C for 6 h, followed by hot isostatic pressing (HIPing) treatment at 1310 °C and 180 MPa for 2 h to produce samples with varied compositions.

Table 1: Average grain size and $\text{SrAl}_{12}\text{O}_{19}$ platelet aspect ratio in ZTA with different contents of SrO derived from SrCO_3 and $\text{Sr}(\text{NO}_3)_2$.

Sample	Average grain size		
	Al_2O_3 (μm)	ZrO_2 (μm)	Aspect Ratio of $\text{SrAl}_{12}\text{O}_{19}$ Platelet
ZTA	0.52±0.22	0.23±0.10	-
ZTA-SC25	0.49±0.23	0.22±0.10	8.9±1.4
ZTA-SC50	0.45±0.22	0.20±0.09	7.3±1.0
ZTA-SC75	0.41±0.22	0.18±0.09	6.2±1.0
ZTA-SC10	0.39±0.19	0.17±0.11	5.6±1.0
ZTA-SN25	0.47±0.20	0.21±0.10	9.2±1.2
ZTA-SN50	0.43±0.21	0.19±0.09	7.6±1.0
ZTA-SN75	0.38±0.20	0.17±0.10	6.4±1.0
ZTA-SN10	0.36±0.18	0.15±0.10	5.7±1.0

(2) Characterization

The sintering density was estimated based on the Archimedes principle. The relative density was calculated by comparing the sintering density of the composite material with the theoretical density. The theoretical densities of α - Al_2O_3 , ZrO_2 , and $\text{SrAl}_{12}\text{O}_{19}$ are 3.98 g/cm³, 6.02 g/cm³ and 3.95 g/cm³, respectively. The phase composition was determined using X-ray diffraction (XRD, D8 ADVANCE, Germany). The thermally etched surface micrographs of the sintered pellets and the analysis of chemical composition were obtained with scanning electron microscopy (SEM, Hitachi S-4800, Japan). The average grain size of the ceramics was determined using the average linear intercept method with Nano Measurer software, which involves measuring the length of randomly selected line segments intersecting grains and calculating an average value to

estimate the mean grain size. The Vickers hardness (H_v) and fracture toughness (K_{IC}) of the composite material were evaluated by means of a microhardness tester (TUKON-2100B, Instron Co., USA) with the application of the 98 N load. The fracture toughness was determined using Eq. (1) derived by Anstis *et al.*²⁰:

$$K_{IC} = 0.016 (E/H)^{1/2} (P/C^{3/2}) \quad (1)$$

where E is the Young's modulus (GPa) of the composite material calculated according to the compositions of the mixtures, H is the Vickers microhardness (GPa), P is the applied load (N), and C is half of the average crack length. The hardness and fracture toughness data were based on the average of five measurements for each sample. When the fracture toughness of ceramic materials is evaluated, results can vary significantly depending on the measurement method. In this paper, the indentation fracture toughness method was employed to facilitate comparisons with most existing literature data.

The flexural strength was measured with the four-point flexural method. Specimens with dimensions of $45 \times 4 \times 3 \text{ mm}^3$ were prepared according to ISO 6474-2. Subsequently, the specimens were loaded on a four-point flexural fixture of a universal testing machine (Instron-5566, Instron Co., USA) with an upper span of 20 mm and a lower span of 40 mm at a crosshead speed of 0.5 mm/min. The flexural strength data were collected as the average of ten measurements per sample.

The Weibull modulus and fracture probability of the material were statistically analyzed based on testing of the three-point fracture strength of 20 specimens measuring $45 \times 4 \times 3 \text{ mm}^3$. The span was 30 mm, and the load was applied at a rate of 0.5 mm/min. The Weibull stress distribution function is shown in Eq. (2):

$$P_f = 1 - \exp(-(\sigma/\sigma_0)^m) \quad (2)$$

where P_f is the fracture probability, σ_0 represents the characteristic fracture strength according to Weibull, σ is the measured fracture strength, and m is the Weibull modulus.

III. Results and Discussion

(1) Phase analysis

The XRD patterns of the ZTA ceramics with different SrO contents are shown in Fig. 1. The diffraction peaks corresponding to tetragonal zirconia phase and alumina phase in the SrO-added ZTA ceramics were consistent with those of $t\text{-ZrO}_2$ (PDF#04-001-7278) and $\alpha\text{-Al}_2\text{O}_3$ (PDF#04-002-5941), respectively. No diffraction peaks corresponding to other zirconia phases ($m\text{-ZrO}_2$ or $c\text{-ZrO}_2$) were found, indicating that the addition of SrO did not impact the crystal structure of tetragonal zirconia. Moreover, no diffraction peaks corresponding to any strontium zirconate phases (such as SrZrO_3 , Sr_3ZrO_7 , or Sr_2ZrO_4) were observed²¹⁻²².

In the ZTA ceramics, the only detected reaction product phase was strontium hexaaluminate ($\text{SrAl}_{12}\text{O}_{19}$, PDF#04-002-2675). The reaction between SrO and Al_2O_3 occurred in two stages. First, SrO reacted with Al_2O_3 to form SrAl_2O_4 when the temperature increased from 900 °C to 1100 °C. Then, SrAl_2O_4 reacted with Al_2O_3 when the temperature increased from 1100 °C to 1400 °C, resulting in the formation of $\text{SrAl}_{12}\text{O}_{19}$. The XRD pattern did not exhibit any diffraction peaks corresponding to other strontium aluminum oxides or SrO. This result indicated that under the present experimental conditions, SrO completely reacted with Al_2O_3 to yield $\text{SrAl}_{12}\text{O}_{19}$, as shown by Eq. (3), which agreed with the previous literature²³.



The formation of the $\text{SrAl}_{12}\text{O}_{19}$ phase was solely dependent on the quantity of added SrO, and the intensity of its diffraction peak significantly increased with the increase in SrO content. Moreover, SrO precursors (such as SrCO_3 and $\text{Sr}(\text{NO}_3)_2$) did not significantly influence the intensity of the $\text{SrAl}_{12}\text{O}_{19}$ diffraction peak.

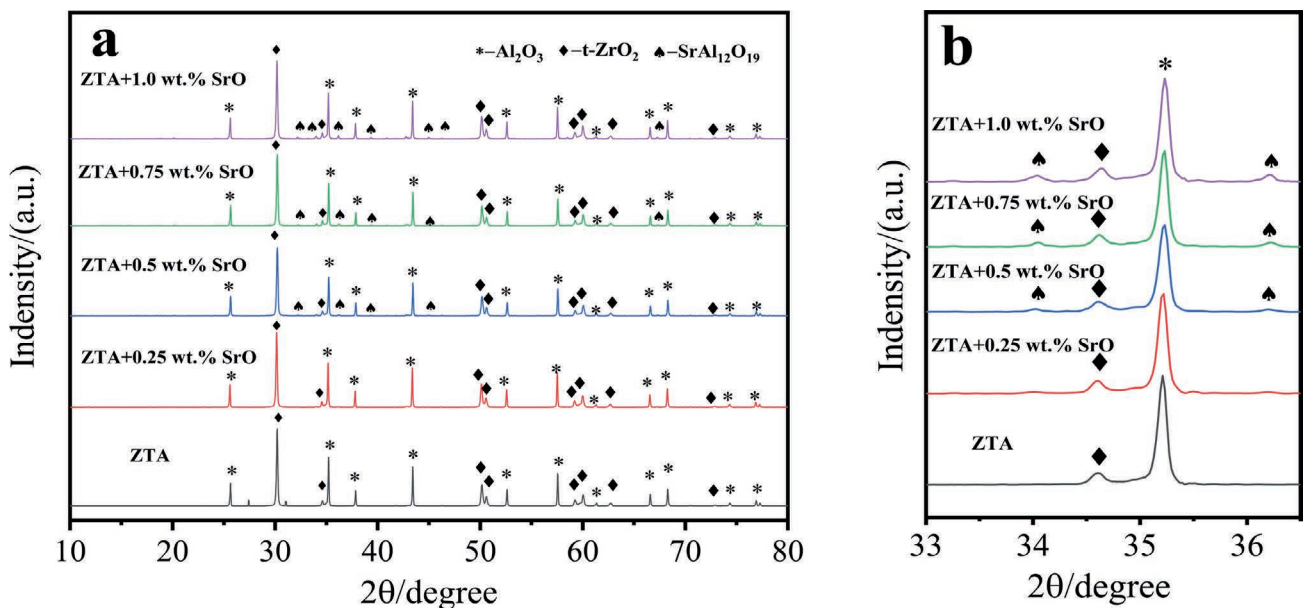


Fig. 1: XRD patterns of ZTA samples with different contents of SrO additive. (a) $2\theta = 10-80^\circ$, (b) $2\theta = 33-36.5^\circ$.

(2) Density and closed porosity

Fig. 2 shows a comparison of the relative density and bulk density between pure ZTA ceramics and ZTA ceramics with different added contents of SrCO_3 and $\text{Sr}(\text{NO}_3)_2$ after pressureless sintering at 1410°C for 6 h. The results indicated that the relative density of pure ZTA was approximately 98.5%. With the increase in SrO content from 0.25 wt% to 1.0 wt%, both the relative density and bulk density of all the samples decreased. Specifically, the relative densities of ZTA-SC10 and ZTA-SN10 decreased to 95.8% and 96.4%, respectively, indicating that the presence of more SrO hindered the densification process of the ZTA ceramics. During the early and middle stages of sintering, SrO was distributed as a secondary phase within the ZTA ceramics, impeding grain boundary migration and grain growth. In the later stages of sintering, SrO gradually reacts with Al_2O_3 , resulting in the formation of elongated $\text{SrAl}_{12}\text{O}_{19}$ platelets. These platelets acted as a secondary phase and further inhibited the densification of the ZTA ceramics^{23–24}. The density data showed that SrO derived from $\text{Sr}(\text{NO}_3)_2$ exhibited a reduced hindering effect on the densification of ZTA compared to SrO derived from SrCO_3 . This discrepancy could be attributed to the powder characteristics of SrO, which is further discussed in respect of the microstructure.

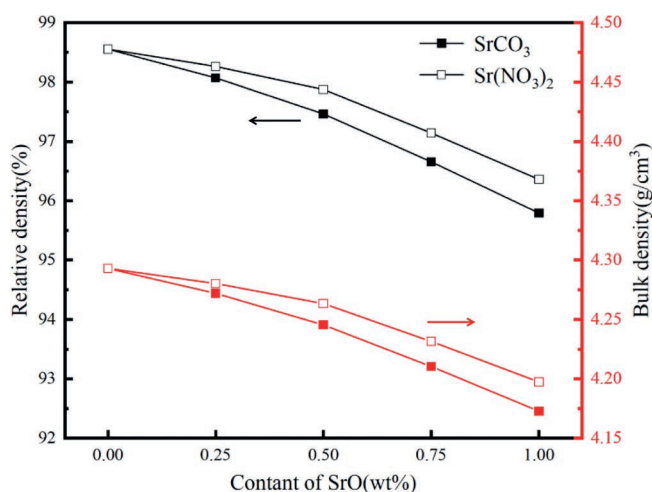


Fig. 2: Bulk density and relative density of pure ZTA and ZTA with different contents (0.25–1.0 wt%) of SrO derived from the SrCO_3 and $\text{Sr}(\text{NO}_3)_2$ additives sintered at 1410°C for 6 h.

Fig. 3 compares the closed porosities of pure ZTA ceramics and ZTA ceramics doped with different contents of SrCO_3 and $\text{Sr}(\text{NO}_3)_2$ after pressureless sintering at 1410°C and HIPing at 1310°C . After pressureless sintering, the porosity of the samples gradually increased with increasing SrO content. When SrO content reached 1.0 wt%, the closed porosities of the ZTA-SC10 and ZTA-SN10 reached 4.1% and 3.6%, respectively. The application of HIPing at 1310°C significantly decreased the porosity of the ceramics. For samples with a SrO content less than 0.5 wt%, the closed porosity was nearly zero, signifying that many closed pores in these samples were situated at grain boundaries and could be effectively eliminated by means of HIPing. When the SrO content surpasses 0.5 wt%, the closed porosity cannot be fully

eliminated, and 0.15% porosity remains. Notably, with a SrO content of 1.0 wt%, a substantial disparity in closed porosity was observed between the two samples: ZTA-SN10 had a porosity of 0.24%, while ZTA-SC10 had a porosity of 0.43%. This difference was likely caused by two factors: 1) As the SrO content increased, the number of $\text{SrAl}_{12}\text{O}_{19}$ platelets subsequently increased, leading to the formation of closed pores at their intersections. Despite these pores located at the intergranular area, they still remained after HIPing. Compared to ZTA-SC10 ceramics, ZTA-SN10 ceramics exhibited a more uniform distribution of $\text{SrAl}_{12}\text{O}_{19}$ platelets, resulting in a reduced occurrence of closed pores at the platelet intersections. 2) The inclusion of SrO during the pressureless sintering process impeded densification, resulting in the creation of more pores. The regions where SrO aggregated had a more pronounced inhibitory effect on the migration of the material, which led to a higher number of closed pores in ZTA-SC10 ceramics.

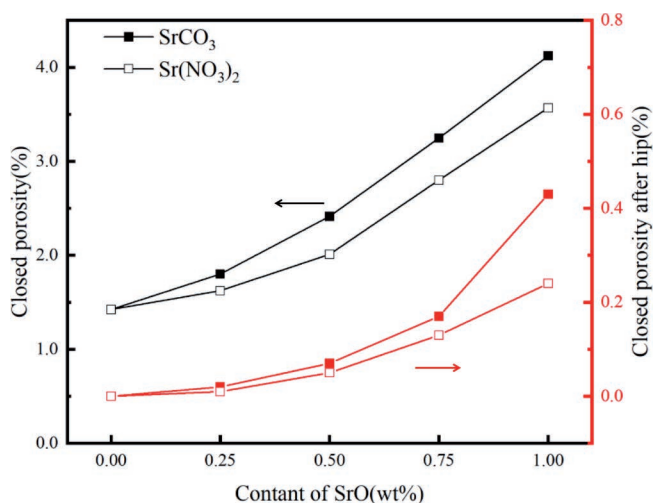


Fig. 3: Close porosity and closed porosity after HIPing of pure ZTA and ZTA with different contents (0.25–1.0 wt%) of SrO derived from SrCO_3 and $\text{Sr}(\text{NO}_3)_2$.

(3) Grain size

The average grain sizes of Al_2O_3 and ZrO_2 are listed in Table 1. It can be seen that the Al_2O_3 and ZrO_2 grain size both decreased as the SrO content increased. Notably, SrO from $\text{Sr}(\text{NO}_3)_2$ had a more pronounced impact on suppressing grain growth. For example, the grain size of Al_2O_3 in the ZTA-SN50 sample ($0.43 \pm 0.21 \mu\text{m}$) was smaller than that in the ZTA-SC50 sample ($0.45 \pm 0.22 \mu\text{m}$). Similarly, the grain size of ZrO_2 in ZTA-SN50 ($0.19 \pm 0.09 \mu\text{m}$) was slightly smaller than that in ZTA-SC50 ($0.20 \pm 0.09 \mu\text{m}$). Based on the analysis of the average grain size and distribution, the SrO derived from $\text{Sr}(\text{NO}_3)_2$ more effectively inhibited the growth of Al_2O_3 and ZrO_2 grains. The observed dependencies could be attributed to the implementation of two mechanisms. First, the segregation of Sr^{2+} ions along the grain boundaries of alumina restricted the diffusion of Al^{3+} and O^{2-} ions, leading to the formation of a fine-grained structure. Second, the synthesis of $\text{SrAl}_{12}\text{O}_{19}$ occurred

due to the reaction between the SrO and Al₂O₃ particles. Therefore, a small portion of the Al₂O₃ was consumed for the forming of SrAl₁₂O₁₉ platelets, accompanied by a decrease in grain size^{23,25}.

The changes in the aspect ratio of SrAl₁₂O₁₉ platelets are also summarized in Table 1; the aspect ratio showed a decreasing trend with increasing SrO content. With the same SrO content, the platelets in the ceramics with added Sr(NO₃)₂ exhibited a slightly higher aspect ratio than those with SrCO₃. For example, SrAl₁₂O₁₉ mainly grew along the basal plane²⁶⁻²⁷, where a low concentration of SrO facilitated complete reaction with adjacent Al₂O₃, resulting in platelet formation. However, aggregation of SrO led to a deficiency of Al₂O₃ along the longitudinal axis of SrAl₁₂O₁₉ platelets and the SrO continued to react with the Al₂O₃ in the transverse direction of the SrAl₁₂O₁₉ platelets to make the platelets grow gradually towards the transverse direction.

(4) Microstructure

SEM images of the polished surfaces of the ZTA ceramics doped with SrCO₃ and Sr(NO₃)₂ (samples ZTA-SC50 and ZTA-SN50) after thermal etching are shown in Fig. 4. In the ZTA-SC50 sample (Fig. 4a), some nonplatelet SrAl₁₂O₁₉ was observed (highlighted in blue), and the number of platelets was relatively small and unevenly

distributed. In contrast, the ZTA-SN50 sample (Fig. 4b) had more platelets with a higher aspect ratio and more uniform distribution. These results indicated that the SrO particles derived from Sr(NO₃)₂ were smaller and exhibited better dispersion and uniformity. On the other hand, the SrO particles derived from SrCO₃ showed some degree of aggregation, which could lead to the formation of nonplatelet strontium aluminum compounds when it reacted with Al₂O₃.

EDS images of nonplatelet strontium aluminum compounds in the ZTA-SC50 sample are shown in Fig. 5. EDS showed that the light gray region was an accumulation area of Sr and Al, with almost no Zr. The region of nonplatelet was an aggregation of platelet SrAl₁₂O₁₉, and the pores were present within the grains and at the grain boundaries. According to Fig. 2, the closed porosity of the ceramics significantly increased with increasing SrO content. The aggregation of SrO in samples with SrCO₃ as an additive was greater than that with Sr(NO₃)₂, resulting in more nonplatelet SrAl₁₂O₁₉ and pores that could not be removed. Consequently, the ZTA-SC series samples had higher closed porosities after HIPing than the ZTA-SN series samples. These findings agreed with the hypothesis presented by R.A. Cutler *et al.*²⁹ that the influence of density reduction could be linked to the uneven distribution of the SrO dopant within the material structure.

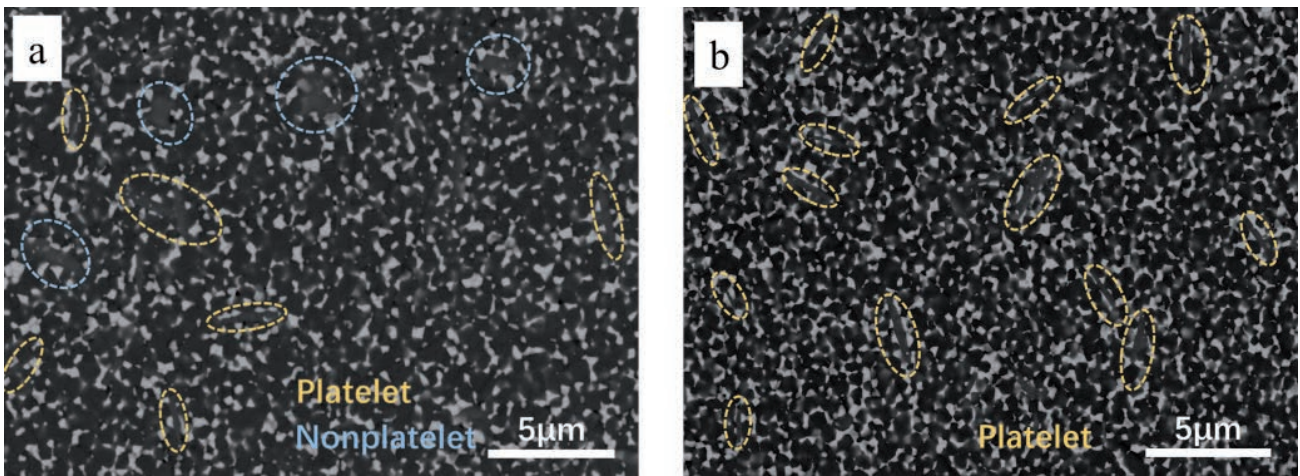


Fig. 4: SEM images of the thermally etched surfaces of (a) ZTA-SC50 and (b) ZTA-SN50.

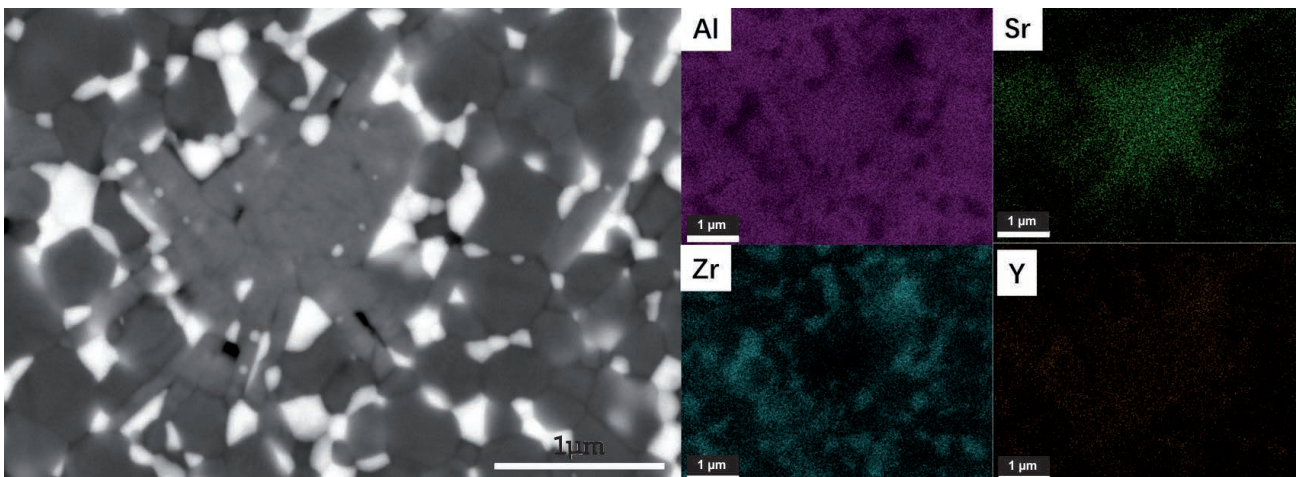


Fig. 5: EDS analysis of the polished surfaces of ZTA-SC50.

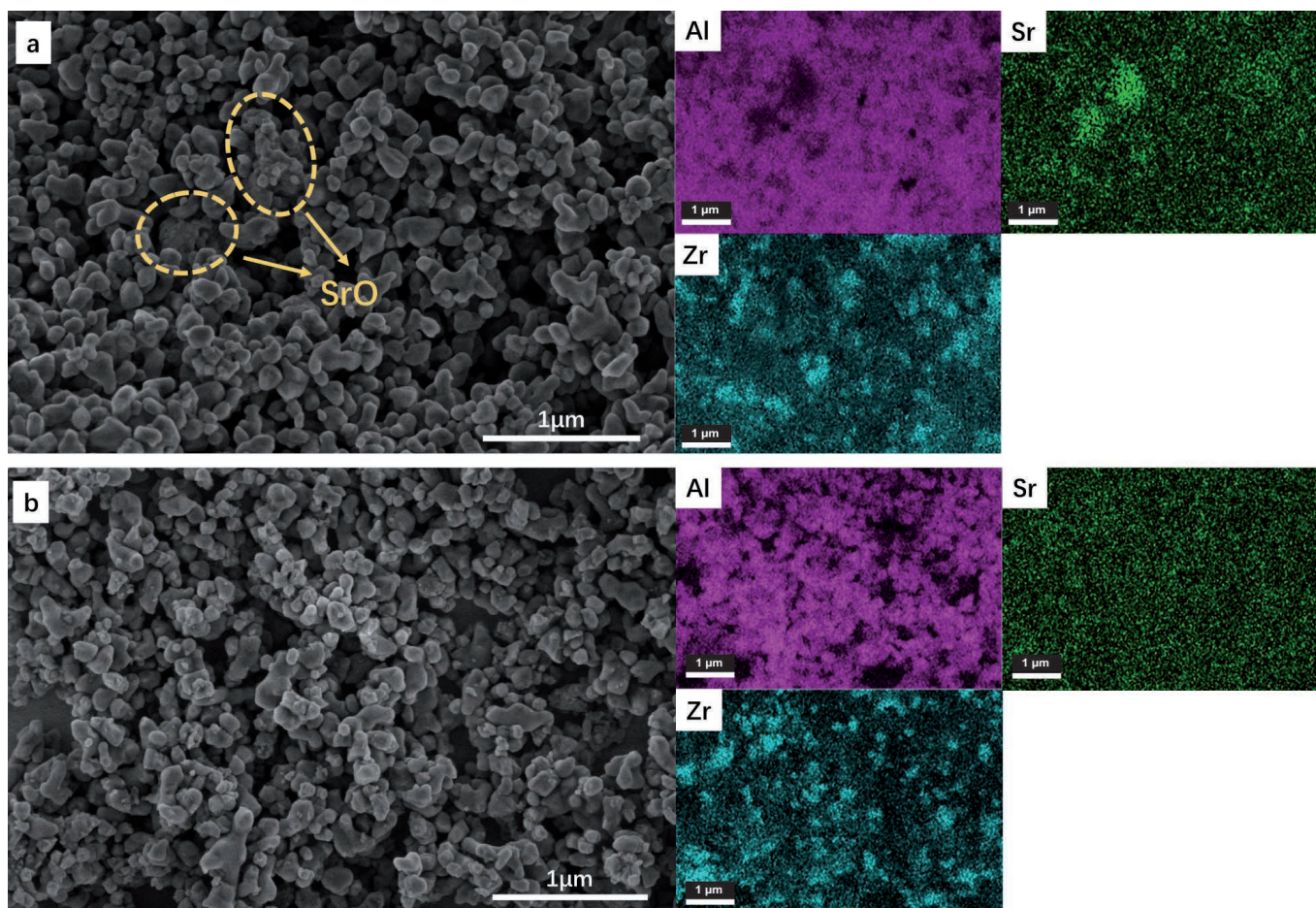


Fig. 6: EDS analysis of (a) ZTA-SC50 and (b) ZTA-SN50 powders.

To determine the uniformity of the distribution of SrO formed from different precursors, EDS mapping was applied. The EDS images of the powders after calcination at 850 °C for ZTA-SC50 and ZTA-SN50 are shown in Fig. 6. It is clear that SrO aggregated in the powder of ZTA-SC50, while SrO was evenly distributed in the powder of ZTA-SN50. These results indicated that the uniformity of the SrO in the ceramic powder derived from $\text{Sr}(\text{NO}_3)_2$ were better than that from SrCO_3 . The reason was that $\text{Sr}(\text{NO}_3)_2$ can slightly dissolve in isopropanol, ionizing into Sr^{2+} and NO_3^- ions, which are evenly distributed in the powder. We speculated that during the powder drying process, as the solvent evaporates, the ion concentration in the solution gradually increases, exceeding the solubility limit under the current conditions. This supersaturated state caused ions to precipitate small and uniform $\text{Sr}(\text{NO}_3)_2$ particles on the surface of the Al_2O_3 and ZrO_2 powders. In contrast, SrCO_3 is insoluble in the solvent after mechanical mixing, and its distribution is not as uniform as that of $\text{Sr}(\text{NO}_3)_2$. The aggregation of SrO contributed to the differences in density, porosity, microstructure, and mechanical properties of the ZTA ceramics.

(5) Mechanical property analysis

Fig. 7a shows a comparison of the hardnesses of pure ZTA ceramics and ZTA ceramics with different contents of SrCO_3 and $\text{Sr}(\text{NO}_3)_2$ after HIPing at 1310 °C. The

fluctuation in the hardness values for ZTA with SrO did not exhibit a clear trend. Hardness is influenced by various factors, such as grain size, internal stress, and pore quantity^{25–27}. The decrease in hardness observed in ZTA-SC25 and ZTA-SN25 was possibly attributed to the inherently lower hardness of $\text{SrAl}_{12}\text{O}_{19}$ compared to that of Al_2O_3 . Conversely, an increase in hardness was observed in ZTA-SC50 and ZTA-SN50 due to the presence of finer grains, a maximum of 18.46 GPa appeared in ZTA-SC50. The highest hardness values were attained through the combination of a fine grain structure and a high relative density. The subsequent decrease in hardness was likely associated with a lower relative density because of the increase of $\text{SrAl}_{12}\text{O}_{19}$ generation.

Fig. 7b compares the fracture toughness of ZTA ceramics with and without SrO from SrCO_3 and $\text{Sr}(\text{NO}_3)_2$ after HIPing at 1310 °C. ZTA ceramics without SrO had a fracture toughness of 5.99 $\text{MPa}\cdot\text{m}^{1/2}$. With the increase in SrO content from 0.25 wt% to 1.0 wt%, fracture toughness was improved for all the samples. Notably, fracture toughnesses of ZTA-SC10 and ZTA-SN10 increased to 6.84 $\text{MPa}\cdot\text{m}^{1/2}$ and 6.97 $\text{MPa}\cdot\text{m}^{1/2}$, showing enhancements of 14.2% and 16.4%, respectively. These results indicated that increasing SrO contributed to enhancing the fracture toughness of ZTA ceramics. In contrast to the trend in fracture toughness, the flexural strength of both types of samples (Fig. 7c)

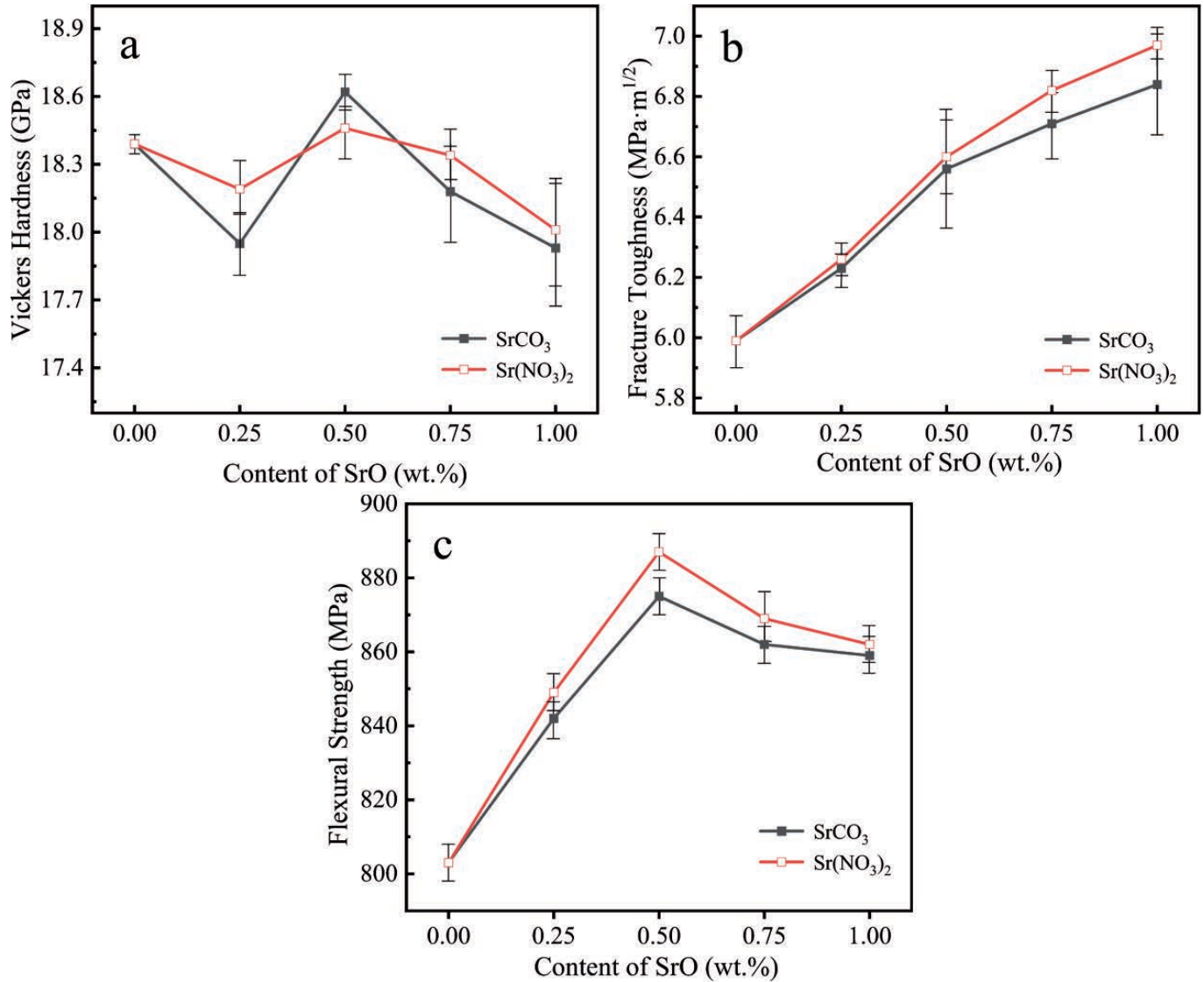


Fig. 7: (a) Vickers hardness, (b) fracture toughness and (c) flexural strength of ZTA with different contents of SrO derived from SrCO₃ and Sr(NO₃)₂.

first increased and then decreased with increasing SrO content. The highest flexural strength was achieved in ZTA-SC50 and ZTA-SN50, reaching 875 MPa and 887 MPa, respectively. The *in situ* formation of SrAl₁₂O₁₉ platelets promoted crack deflection and bridging along grain boundaries, increasing the fracture energy, which has been widely reported in the literature^{5–8,29}. Additionally, the fine-grained structure significantly enhanced the ceramic's fracture toughness and flexural strength. However, with a further increase in SrO content, ceramic density decreased, leading to a decrease in the flexural strength. Compared to those with SrCO₃, the fracture toughness and flexural strength of the ZTA ceramics with Sr(NO₃)₂ were higher, which was attributed to the more uniform distribution and higher aspect ratio of the SrAl₁₂O₁₉ platelets. Conversely, the addition of SrCO₃ increased the number of nonplatelet SrAl₁₂O₁₉, resulting in additional defects and reducing both the fracture toughness and flexural strength.

To explain the differences more intuitively in the distribution of SrAl₁₂O₁₉ platelets in ZTA ceramics due to

two different precursors, three-point fracture strength tests were conducted on the ZTA-SC50 and ZTA-SN50 samples, and the Weibull modulus and fracture probability were statistically analyzed. Fig. 8 compares the Weibull modulus of the ZTA-SC50 and ZTA-SN50 samples. The Weibull modulus of the ZSC50 sample is 19.77, while that of the ZTA-SN50 sample is higher, at 20.19. The Weibull modulus is an important method for evaluating the reliability of ceramics; a higher Weibull modulus indicates better homogeneity of the phase distribution, fewer defects, and higher reliability. The higher Weibull modulus of the ZTA-SN50 sample suggests a more uniform distribution of SrAl₁₂O₁₉ platelets in the ZTA-SN50 sample compared to the ZTA-SC50 sample, with fewer defects. Fig. 9 shows the fracture probability plots for the ZTA-SC50 and ZTA-SN50 samples. From the figure, it is evident that with increasing fracture strength, the fracture probability of the ZTA-SN50 sample is significantly lower than that of the ZTA-SC50 sample, indicating fewer defects caused by the aggregation of SrAl₁₂O₁₉ platelets

in the ZTA-SN50 sample and thus higher reliability of the ZTA-SN50 sample.

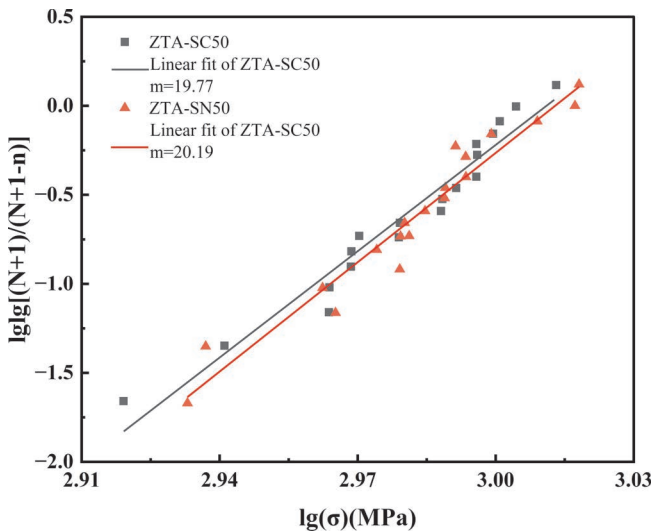


Fig. 8: Weibull modulus of ZTA-SC50 and ZTA-SN50.

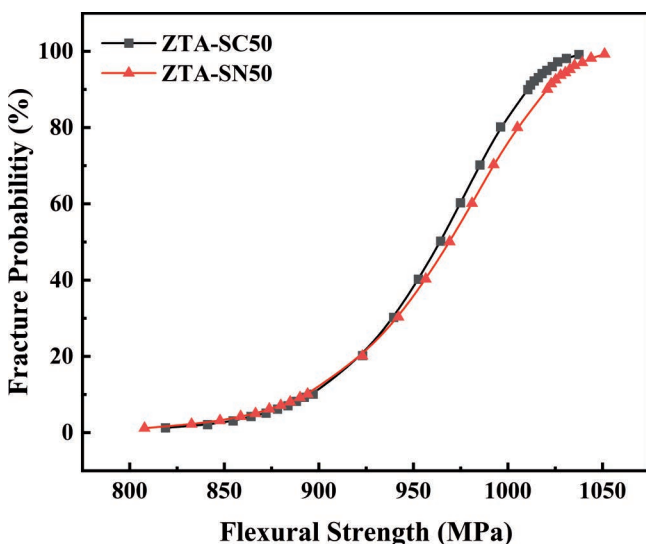


Fig. 9: Fracture probability of ZTA-SC50 and ZTA-SN50.

IV. Conclusions

The effect of SrO from SrCO_3 and $\text{Sr}(\text{NO}_3)_2$ additives on the microstructure and mechanical properties of ZTA was evaluated. SrO inhibited the densification process and grain growth of the ZTA ceramics while simultaneously generating $\text{SrAl}_{12}\text{O}_{19}$ platelet *in situ*. Compared to SrO derived from SrCO_3 , SrO derived from $\text{Sr}(\text{NO}_3)_2$ exhibits a more uniform distribution and more effectively suppresses the growth of Al_2O_3 and ZrO_2 grains. ZTA ceramics with $\text{Sr}(\text{NO}_3)_2$ exhibited excellent fracture toughness and flexural strength, which was attributed to a more uniform platelet distribution with a higher aspect ratio. After pressureless sintering at 1410 °C for 6 h and HIPing at 1310 °C, the maximum values for the hardness, flexural strength, and fracture toughness of the $\text{Sr}(\text{NO}_3)_2$ -added ZTA ceramics were 18.46 GPa, 887 MPa, and 6.97 $\text{MPa}\cdot\text{m}^{1/2}$, respectively. These results demon-

strated that using nitrates as SrO precursor is an effective method to promote uniform distribution of SrO and then improve the mechanical properties of ZTA ceramics.

Acknowledgments

This work was supported by the National Natural Science Foundation of China (Grant No. U23A20564).

Declaration of competing interest

The authors have no competing interests to declare that are relevant to the content of this article.

References

- Li, B.S., Huang, J.X., Guo, J.K., Yan, D.S.: Studies on mechanical properties and toughening mechanism of tetragonal zirconia polycrystals, *J. Inorg. Mater.*, **1**, [2], 129–134, (1986).
- Manshor, H., Abdullah, E.C., Azhar, A.Z.A., Sing, Y.W., Ahmad, Z.A.: Microwave sintering of zirconia-toughened alumina (ZTA)- TiO_2 - Cr_2O_3 ceramic composite: the effects on microstructure and properties, *J. Alloy. Compd.*, **722**, 458–466, (2017).
- Mangalaraja, R.V., Chandrasekhar, B.K., Manohar, P.: Effect of ceria on the physical, mechanical and thermal properties of yttria stabilized zirconia toughened alumina, *Mater. Sci. Eng. A-Struct. Mater. Prop. Microstruct. Process.*, **343**, 71–75, (2003).
- Wu, Y.Q., Zhang, Y.F., Huang, X.X., Guo, J.K.: In-situ growth of needlelike $\text{LaAl}_{11}\text{O}_{18}$ for reinforcement of alumina composites, *Ceram. Int.*, **27**, 903–906, (2001).
- Guo, R., Guo, D., Chen, Y., Yang, Z., Yuan, Q.: In-situ formation of $\text{LaAl}_{11}\text{O}_{18}$ rodlike particles in ZTA ceramics and effect on the mechanical properties, *Ceram. Int.*, **28**, 699–704, (2002).
- Sarath Chandra, K., Monalisa, M., Chowdary, C., Ghosh, G., Sarkar, D.: Microstructure and mechanical behavior of SrO doped Al_2O_3 ceramics, *Mater. Sci. Eng. A*, **739**, 186–192, (2019).
- Li, W., Bai, M.: Effect of PrAlO_3 on mechanical properties of zirconia toughened alumina bioceramics after hydrothermal aging, *J Chin Ceram Soc.*, **51**, 721–729, (2023).
- Sktani, Z.D.I., Arab, A., Mohamed, J.J., Ahmad, Z.A.: Effects of additives additions and sintering techniques on the microstructure and mechanical properties of zirconia toughened alumina (ZTA): a review, *Int. J. Refract. Met. Hard Mat.*, **106**, (2022).
- Sánchez-Herencia, A.J., Moreno, R., Baudín, C.: Fracture behavior of alumina-calcium hexaluminate composites obtained by colloidal processing, *J. Eur. Ceram. Soc.*, **20**, 2575–2583, (2000).
- Chen, P.L., Chen, I.W.: In-situ alumina/aluminate platelet composites, *J. Am. Ceram. Soc.*, **75**, 2610–2612, (1992).
- An, L., Chan, H.M.: R-curve behavior of in situ-toughened Al_2O_3 : $\text{CaAl}_{12}\text{O}_{19}$ ceramic composites, *J. Am. Ceram. Soc.*, **79**, 3142–3148, (1996).
- Vishista, K., Gnanam, F.D.: Effect of strontia on the densification and mechanical properties of sol-gel alumina, *Ceram. Int.*, **32**, 917–922, (2006).
- An, L., Chan, H.M., Soni, K.K.: Control of calcium hexaluminate grain morphology in in-situ toughened ceramic composites, *J. Mater. Sci.*, **31**, 3223–3229, (1996).
- Luan, L., Guo, C.F., Huang, D.X.: Effect of Al/Sr ratio on properties of strontium aluminate long lasting phosphor, *J. Inorg. Mater.*, **24**, 53–56, (2009).

- 15 Jiang, S., Yang, J., Sun, Y.: Effect of Cr_2O_3 on microstructure and mechanical properties of SrO-ZTA composite ceramics, *Journal of Ceramics*, **45**, [4], 720–728, (2024).
- 16 Arab, A., Ahmad, R., Ahmad, Z.A.: Effect of SrCO_3 addition on the dynamic compressive strength of ZTA, *Int. J. Miner. Metall. Mater.*, **23**, 481–489, (2016).
- 17 Naga, S.M., Shaer, M.E., Awaad, M., Saleh, M.A.: Effect of soaking time on the properties of $\text{SrAl}_{12}\text{O}_{19}$ /ZTA composites, *J. Mater. Eng. Perform.*, **29**, 2920–2925, (2020).
- 18 Naga, S.M., Elshaer, M., Awaad, M., Amer, A.A.: Strontium hexaaluminate/ZTA composites: preparation and characterization, *Mater. Chem. Phys.*, **232**, 23–27, (2019).
- 19 Basha, S.A., Chandra, K.S., Sarkar, D.: Salient features of SrO doping in Al_2O_3 -5 wt.% ZrO_2 reaction sintered ceramic composites, *J. Alloy. Compd.*, **829**, (2020).
- 20 Anstis, G.R., Chantikul, P., Lawn, B.R., Marshall, D.B.: A critical evaluation of indentation techniques for measuring fracture toughness: 1. direct crack measurements, *J. Am. Ceram. Soc.*, **64**, 533–538, (1981).
- 21 Noguchi, T., Okubo, T., Yonemochi, O.: Reactions in the system ZrO-SrO, *J. Am. Ceram. Soc.*, **52**, 178, (1969).
- 22 Naga, S.M., Elshaer, M., Awaad, M., Amer, A.A., Strontium hexaaluminate/ZTA composites: preparation and characterization, *Mater. Chem. Phys.*, **232**, 23–27, (2019).
- 23 Kuzmin, R., Cherkasova, N., Bataev, A.: Strontium hexaaluminate formation in alumina and alumina-zirconia matrixes, *Ceram. Int.*, **47**, 6854–6859, (2021).
- 24 Vishista, K., Gnanam, F.D.: Microstructural development of $\text{SrAl}_{12}\text{O}_{19}$ in alumina-strontia composites, *J. Eur. Ceram. Soc.*, **29**, 77–83, (2009).
- 25 Sktani, Z.D.I., Azhar, A.Z.A., Ratnam, M.M., Ahmad, Z.A.: The influence of in - situ formation of hibonite on the properties of zirconia toughened alumina (ZTA) composites, *Ceram. Int.*, **40**, 6211–6217, (2014).
- 26 DomÍnguez, C., Chevalier, J., Torrecillas, R., Fantozzi, G.: Microstructure development in calcium hexaluminate, *J. Eur. Ceram. Soc.*, **21**, 381–387, (2001).
- 27 Inoue H., Sekizawa K., Eguchi K., Arai H.: Changes of crystalline phase and catalytic properties by cation substitution in mirror plane of hexaaluminate compounds, *J. Solid State Chem.*, **121**, 190–196, (1996).
- 28 Gardner T.H., Shekhawat D., Berry D.A.: Effect of nickel hexaaluminate mirror cation on structure-sensitive reactions during n -tetradecane partial oxidation, *Appl. Catal. A-Gen.*, **323**, 1–8, (2007).
- 29 Cutler R.A., Lindemann J.M., Ulvensøen J.H.: Damage-resistant SrO-doped Ce-TZP/ Al_2O_3 composites, *Materials & Design*, **15**, [3], 123–133, (1994).

